Ann. Phys. (Leipzig) **13**, No. 7–8, 391 – 402 (2004) / **DOI** 10.1002/andp.200410082

Transverse pattern formation and its control in photorefractive optics

C. Denz[1,*], **Ph. Jander**[1], **M. Schwab**[1,**], **O. Sandfuchs**[2,***], **M. Belić**[3,****], and **F. Kaiser**[2]

[1] Institute of Applied Physics, Westfälische Wilhelms-Universität Münster, 48149 Münster, Germany
[2] Institute of Applied Physics, Darmstadt University of Technology, 64289 Darmstadt, Germany
[3] Optique Nonlinéaire Théorique, Université Libre de Bruxelles, 1050 Bruxelles, Belgium

Received 16 February 2004, accepted 5 April 2004
Published online 17 June 2004

Key words Pattern formation, photorefractive optics.
PACS 42.65.Hw, 42.65.Sf

This review is dedicated to Prof. Dr. H.-G. Purwins, Institute of Applied Physics, University of Münster, who is always enthousiastically supporting nonlinear sciences.

A wealth of periodic transverse patterns is observed in nonlinear optical, photorefractive single-feedback systems. It is the extension of a photorefractive medium in the direction of propagation of the laser beam that allows for the formation of stable hexagons, squares, rhombuses and dodecagons above the first bifurcation of the system. In this article we review the formation of these periodic patterns and present linear and nonlinear stability analyses that predict the type of pattern to appear. Amplitude equations for the interactions of unstable sidebands are introduced. We compare numerical and experimental results on two-dimensional transverse pattern formation. We present control methods for the invasive and non-invasive manipulation of different pattern states using a Fourier filtering technique.

1 Introduction

Spatiotemporal complexity of nonlinear optical systems is a new and exciting field of research in optics, that has already found way into a number of review papers [1], special issues [2], and books [3,4]. Spatiotemporal patterns arise when the translational symmetry of a homogeneous state is spontaneously broken, induced by transverse coupling due to diffraction in nonlinear optical systems, and can give rise to chaotic dynamics and/or spontaneous pattern formation. The more extended an optical system is in its transverse dimensions, the greater the wealth of different transverse patterns. Among them, periodic structures are predominant for weak nonlinearities, whereas spatial solitons, spatiotemporal dynamics as well as optical turbulence may arise for higher nonlinearities. The existence and stability of these structures is strongly affected by symmetries, both geometric ones due to the optical configuration or intrinsic symmetries of the optical interactions under the influence of material properties.

In photorefractive (PR) optics transverse pattern formation appears predominantly due to two-wave mixing processes in a reflection grating geometry. Under certain circumstances each beam becomes spontaneously unstable against the excitation of satellite beams [5], whose wave vectors belong to a cone in the Fourier space, and whose initial growth is exponential. This growth is arrested either through the depletion of pump beams or through the saturable character of the medium nonlinearity. In the nonlinear stage of

* Corresponding author E-mail: denz@uni-muenster.de
** Present address: Charlottenstr. 39, 70825 Korntal-Münchingen, Germany
*** Present address: Sophienstr. 1, 07743 Jena, Germany
**** Permanent address: Institute of Physics, P.O. Box 57, 11001 Belgrade, Serbia

pattern formation, a finite set of pairs of wave vectors is selected on the ring, leading to specific geometric arrangements that include different patterns.Typically, hexagonal or stripe patterns appear. Symmetries and the type of bifurcation at the threshold determine the form of ensuing primary patterns and the order-parameter equations describing them. At a later stage of pattern organization, after secondary transitions, the patterns may display defects or domain walls. To understand the formation mechanism, techniques to control and manipulate transverse patterns are of huge importance. One of the major challenges in this area is to implement control methods that allow the pattern forming system to remain nearly unchanged, and at the same time perform efficient pattern selection. These topics comprise the contents of this review.

The paper is structured as follows. Sect. 2 introduces the geometry in which pattern formation is studied in nonlinear PR systems. Sect. 3 presents the PR effect and wave mixing in PR media, necessary for understanding the nonlinearity that causes the pattern formation process. Sect. 4 is concerned with the model equations and the linear stability analysis, whereas Sect. 5 deals with the nonlinear dynamical analysis and amplitude equations formalism describing patterns. In Sect. 6, numerical simulations and experimental results are presented, with an emphasis on the competition and dynamics of different patterns. Finally, Sect. 7 introduces the concept of manipulation and control of patterns, and demonstrates a minimally-invasive technique to select different pattern in an optical feedback system.

2 Pattern forming geometry

The field of pattern formation in PR optics effectively started in 1993, with a remarkable series of experiments by T. Honda and coworkers [6–8]. Using the basic geometry for spontaneous pattern formation in nonlinear optical media – that of wave mixing of two counterpropagating beams created by a single feedback mirror – they not only observed the basic hexagonal pattern, but also noted both positive (H^+) and negative (H^-)hexagons. Moreover, they presented the first linear stability analysis, and found the threshold condition for pattern formation [9]. Soon followed the observation of patterns other than hexagons, mostly unstable or in competition with hexagons: stripes [10], squares and squeezed hexagons [11,12], and even quasi-periodic patterns involving dodecagons. This has been made possible by utilizing the virtual mirror concept [11,13], which projects the feedback mirror virtually back into the crystal with the help of a 4f-configuration of imaging lenses in the feedback arm. This allows access to the parameter region where different, non-hexagonal pattern and pattern competition [14, 15] can be found. Later, to stabilize or select different patterns, use has been made of Fourier control techniques in different feedback configurations [13,16–18] and of frequency-selective techniques [19].

A typical experimental setup is presented in Fig. 1 [3]. A frequency-doubled Nd:YAG-laser at $\lambda = 532\,\mathrm{nm}$, operating at several 10 mW, is used as the laser source. A single mirror feedback arrangement is utilized, supplemented by two lenses forming a 4f imaging system within the feedback loop. The PR medium of choice is an iron-doped potassium niobate crystal, which is chosen for its large effective electro-optic coefficient and low noise at the wavelength of Nd:YAG laser emission at 532 nm. To reduce reflections from the back side of the material, the c-axis of the crystal is nearly aligned in the beam propagation direction and oriented in such a way that the incoming, forward propagating beam F is attenuated and the reflected, backward travelling beam B is amplified during the two-wave mixing process in the crystal. If the PR coupling strength is above an instability threshold, the laser beam undergoes a transverse modulation and spontaneous patterns appear. They are visualized using a beam splitter in the far field and a microscope lens system in the near field. Both fields are registered with CCD cameras.

Typical pattern outputs of this standard setup, both experimental and numerical, are depicted in Fig. 2. Due to the strong modulation of the pattern, the near field pattern of the reflected light consists of dark spots arranged on a hexagonal lattice. This is known as the H^- hexagonal pattern. The transmitted pattern on the other face of the crystal is antiphased, and consists of bright spots on a hexagonal lattice – the H^+ pattern. The difference arises from the symmetry-breaking nature of the bifurcation when counterpropagating side-band beams appear. Symmetry breaking and transverse modulational instability lead to antisymmetric patterns

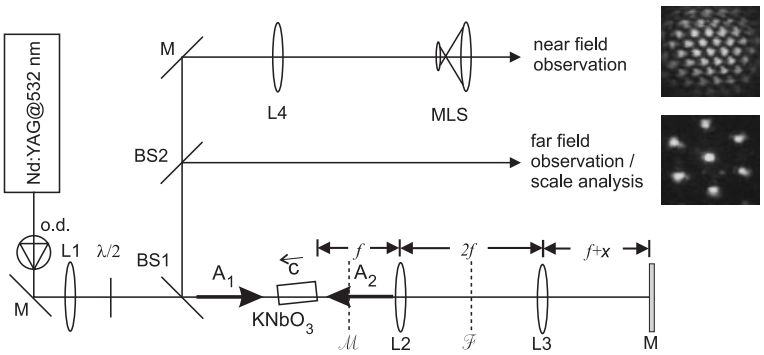

Fig. 1 Experimental setup for the study of PR patterns.The single feedback mirror configuration is given by the PR $KNbO_3$-crystal, the lenses L1 and L2 and the feedback mirror M. Far-field and near-field are visualized by the help of beam splitter BS1, and BS2 and the microscope lens systems MLS, respectively. Feedback of the modulated beam back into the laser is prevented by an optical diode o.d. based on a Faraday rotator.

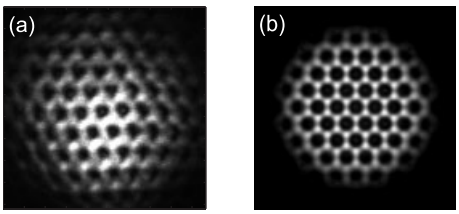

Fig. 2 Honeycomb (H^-) patterns for a mirror position slightly behind the back of the crystal (positive propagation length). (a) Experimental, (b) numerical results of the transverse pattern in two dimensions.

developing in the opposite propagation directions [20]. Such antiphase behavior is a characteristic feature of PR patterns. One can connect the antiphase behavior with the phase-conjugate nature of the wave mixing equations describing the development and interactions of side-band beams.

3 Photorefractive effect

The PR effect represents a photoinduced change in the index of refraction of an electro-optical material. It is observed in a range of materials, including ferroelectric crystals ($LiNbO_3$, $KNbO_3$, $BaTiO_3$, SBN), paraelectric crystals (BSO, BGO), semiconductors (GaAs), and some polymers. It has been discovered accidentally in 1966 [21], and initially considered a nuisance – an 'optical damage'. However, it was soon realized that it can be usefully employed for a number of applications. Today it forms the basis of a whole new field of nonlinear optics, PR optics [22, 23].

The effect itself is quite complex, and proceeds in four main stages. In the first stage – photo-excitation – the charges are excited from donors to the conduction band under the influence of light. In the second, charge transport stage, the mobile charges move away from the illuminated regions, either due to diffusion or drift under the influence of an applied external field, and accumulate in the dark regions, where they are re-trapped by the available acceptors. As a result of charge separation, an electric field builds within the crystal, the so-called space charge field. In the final stage, the space charge field changes the index of refraction via the linear electro-optic effect. The changed index of refraction is of the form

$$\Delta n = -0.5 n_0^3 r_{\text{eff}} E, \tag{1}$$

where n_0 is the crystal bulk refractive index, and r_{eff} is the effective electro-optic coefficient. Experimental systems are usually designed in a way that exploits the largest electro-optic component, for achieving the maximum PR coupling. Because the resulting refractive index modulation in turn strongly influences the light propagation in the material, the geometry of wave mixing is essential for coupling effects. In our

case, two wave mixing via a single reflection grating is used, hence the space charge field will mix the counterpropagating components, and will be proportional to the amplitude of the resulting grating.

A theoretical description of the PR effect is provided by the standard model of Kukhtarev et al. [24]. It consists, quite appropriately, of the equations for the generation/recombination rate of mobile charges, the continuity equation for the current density, and Poisson's equation for the charge density [23]. Kukhtarev's material equations represent a closed system of partial differential equations in space and time.

4 Two wave-mixing in reflection geometry

4.1 Model equations

In a standard two-wave mixing configuration, two beams of the same frequency and opposite k vectors are incident on the crystal. The electric field of the light is a superposition of waves $A_1 \exp(ik_0 z + i\omega t) + A_2 \exp(-ik_0 z + i\omega t) + c.c.$ counter-propagating along the z-direction, where k_0 is the wave vector in the medium and ω the optical frequency. A_1 and A_2 are the slowly varying envelopes of the beams and $c.c.$ stands for complex conjugation. The total light intensity, measured in units of I_b, is given by

$$1 + I = (1 + I_0) \cdot \left(1 + \frac{m}{2} \exp(2k_0 z) + c.c.\right), \tag{2}$$

where $I_0 = |A_1|^2 + |A_2|^2$ is the sum of the beam intensities and $m = 2A_1 A_2^*/(1 + I_0)$ is the modulation depth. The two-wave mixing process is described by the slowly varying envelope paraxial wave equations

$$\partial_z A_1 + \mathrm{i} f \Delta A_1 = -Q A_2, \qquad -\partial_z A_2 + \mathrm{i} f \Delta A_2 = Q^* A_1, \tag{3}$$

where z, the propagation coordinate, is scaled by the crystal thickness L, and f, the diffraction parameter, is proportional to the inverse of the Fresnel number, $f = (4\pi F)^{-1} = L/(2k_0 w_0^2)$. Here, w_0 is the transverse scaling length, typically the beam waist. Δ is the transverse Laplacian, and $Q = \mathrm{i} k_0 L \Delta n / 2n_0$ is the amplitude of the reflection grating, proportional to the modulation depth, whose temporal evolution is described by a relaxation equation of the form

$$\tau(I)\, \partial_t Q + Q = \Gamma \frac{A_1 A_2^*}{1 + I_0}. \tag{4}$$

Here, Γ is the wave coupling constant. In general it is a complex quantity, but can be assumed to be real for the case of a diffusion-dominated charge transport mechanism, which takes place in the commonly used PR crystals $KNbO_3$ and $BaTiO_3$. Eqs. (3) and (4) form the basic model. For further analysis of pattern formation, the assumption is made that the dynamics of the wave envelopes is slaved to the grating amplitude, because of its slow evolution, and that the spatial distribution of Q is determined by the spatial distribution of the beam envelopes.

4.2 Linear stability analysis

A typical threshold curve for modulational instabilities is displayed in Fig. 3(a), as a function of the sideband angle K^2/k_0^2. For most mirror distances there exists a global minimum of the coupling strength ΓL at which one band around a critical transverse K_c becomes unstable. For the mirror distance $D = 0$ and the reflectivity $R = 1$ this happens at $(\Gamma L)_c \approx 3.82$ and $f K_c^2 \approx 2.59$. The values of the threshold coupling strengths as a function of the diffraction length are shown in Fig. 3(b). The virtual mirror concept allows for negative diffraction lengths D and mirror positions within the crystal. The shape of the threshold coupling curves indicates that a whole band of transverse wave vectors becomes unstable around $D = -0.5$, leading to the competition between different patterns. This parameter region coincides with the experimentally found region of multiple pattern stability, where a number of coexisting transverse patterns with different wave vectors is observed and competes dynamically.

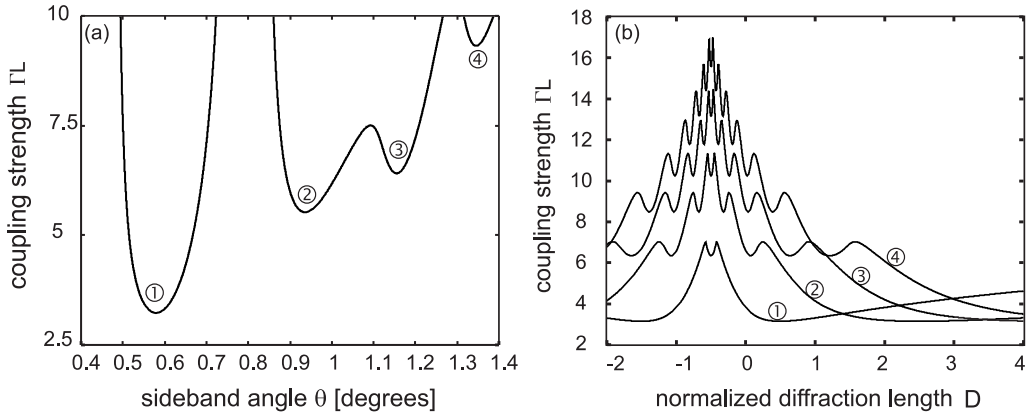

Fig. 3 (a) Threshold curve for $D = 0.6$, as a function of the sideband angle. (b) Critical coupling strengths for different mirror positions, corresponding to the minima in (a).

The linear stability allows for the determination of the primary instability threshold. For PR media it has been discussed in a number of papers [9, 12, 14, 25–27]. It consists in making a small deviation from the homogeneous solution, and solving the linearized eqs. (3) and (4). The coupling constant Γ plays the role of the bifurcation parameter. For given boundary conditions and parameter values, after a certain threshold value of Γ, an instability starts to grow.

5 Nonlinear dynamical analysis and amplitude equations

5.1 Nonlinear analysis

The question which specific pattern can be formed out of the ring of active modes is answered by the nonlinear bifurcation analysis, which consists in making a perturbation around the homogeneous stable solution and analyzing eqs. (3) and (4) for the perturbations, including all nonlinear terms. For the general description of multiple scale analysis it is convenient to choose a real basis for the state vectors of perturbations via a transformation: $(a_1, a_1^*, a_2, a_2^*)^T \longrightarrow \vec{U} = (U_1, U_2, U_3, U_4)^T$ and $(q, q^*)^T \longrightarrow \vec{P} = (P_1, P_2)^T$, which brings the equations for the perturbations into a general form

$$\begin{aligned} \mathcal{L}_{z;x,y}\vec{U} + \mathcal{M}_0\vec{P} &= \vec{\mathcal{M}}_1(\vec{P}|\vec{U}), \\ \left(\mathcal{D}_{0,t} + \mathcal{D}_{1,t}(\vec{U}) + \ldots\right)\vec{P} - \mathcal{N}_0\vec{U} &= \vec{\mathcal{N}}_1(\vec{U}|\vec{U}) + \vec{\mathcal{N}}_2(\vec{U}|\vec{U}|\vec{U}) + \ldots \end{aligned} \tag{5}$$

Here the matrices $\mathcal{L}_{z;x,y}$ and $\mathcal{D}_{j,t}$ are the spatial and temporal derivative operators. The matrices $\mathcal{M}_0$ and $\mathcal{N}_0$ are composed of the coefficients of the linear coupling between the field and the grating, and $\vec{\mathcal{M}}_j$ and $\vec{\mathcal{N}}_j$ are the vectors describing nonlinear field-grating and field-field interactions. The symbols $(\vec{U}|\vec{U})$ and $(\vec{U}|\vec{U}|\vec{U})$ are shorthand notations for different quadratic and cubic terms arising in such a procedure.

The multiple scale analysis is based on the fact that in the neighborhood of a bifurcation point the temporal evolution is separable into fast and slow scales. The PR coupling strength Γ is the bifurcation parameter, and the expansion parameter ε scales the distance from the critical point Γ_c at which the modulational instability starts growing. To describe pattern formation through a Landau-type formalism, one expands the bifurcation parameter Γ, the temporal variable t, the field $\vec{U}$ and the grating amplitudes $\vec{P}$ in powers of ε:

$$\Gamma = \Gamma_c + \varepsilon\Gamma^{(1)} + \varepsilon^2\Gamma^{(2)} + \ldots, \qquad t = T_0 + \varepsilon T_1 + \varepsilon^2 T_2 + \ldots,$$

$$\vec{U} = \varepsilon\vec{U}^{(1)} + \varepsilon^2\vec{U}^{(2)} + \varepsilon^3\vec{U}^{(3)} + \ldots, \qquad \vec{P} = \varepsilon\vec{P}^{(1)} + \varepsilon^2\vec{P}^{(2)} + \varepsilon^{3\nu}\vec{P}^{(3)} + \ldots \tag{6}$$

Even though the terms are grouped in eqs. (5) according to their order in nonlinearity, these equations still describe the evolution of all combinations of modes, and hence all possible patterns. One proceeds to write modal equations at each order of ε, hoping to reach saturation at some finite and low order of nonlinearity. To study a particular pattern, one introduces order parameters $W_j = W_j(T_1, T_2, \ldots)$ which are proportional to the amplitudes of critical modes on the unstable ring. Stationary patterns require that the amplitude W_j belonging to K_c and the amplitude W_j^* belonging to $-K_c$ appear together. So, the mode amplitudes appear in pairs.

In the first order of ε one recovers the linear problem. Higher orders in ε describe the nonlinear interaction of spatial modes and result in the amplitude equation for each of the order parameters [28]. A specific stationary pattern may consist of any combination of N spot pairs on the ring. To determine which of them will result in a stable configuration, one derives the cubic self- and cross-coupling coefficients of all possible mode interactions. Here it is sufficient to calculate the coefficients for bimodal ($N = 2$) and, for the case of a resonant interaction, the coefficients for the trimodal ($N = 3$) interaction.

5.2 Amplitude equations

A bimodal structure consists of two pairs of critical wave vectors, with an angle θ between them. The coupled amplitude equations for the rhombic pattern are of the form:

$$\begin{aligned} \tau_0\, d_t W_1 &= (\Gamma - \Gamma_c)W_1 - \left(g_\pi |W_1|^2 + g_\theta |W_2|^2\right) W_1, \\ \tau_0\, d_t W_2 &= (\Gamma - \Gamma_c)W_2 - \left(g_\pi |W_2|^2 + g_\theta |W_1|^2\right) W_2, \end{aligned} \tag{7}$$

where τ_0 is the relaxation rate, and g_π and g_θ are the self- and cross-coupling coefficients. These are the coupled Landau equations for the rhombic planforms. They provide a universal description for the self-organization of bimodal patterns, which is similar to a second-order phase transition.

In the PR feedback system a resonant interaction occurs between three pairs of critical modes, rotated for $2\pi/3$, resulting in the hexagonal structure. The corresponding amplitude equations are of the form:

$$\tau_0\, d_t W_1 = (\Gamma - \Gamma_c)W_1 - g_\pi |W_1|^2 W_1 - g_{\pi/3}\left(|W_2|^2 + |W_3|^2\right) W_1 + g_H W_2^* W_3^* \tag{8}$$

and analogously for W_2 and W_3 through the cyclic permutation of indices. These are the well-known coupled Landau amplitude equations for hexagonal patterns.

5.3 Stability and coexistence of photorefractive patterns

From the coefficients of bimodal and trimodal interactions it is possible to determine analytically the stability of planforms with any N-modal structure that may occur in the PR feedback system. Among the patterns with $N = 2$ one generically finds that the stripes are stable if $g_\theta > g_\pi$, whereas rhombi are only stable if $g_\theta < g_\pi$. In particular, square patterns ($\theta = \pi/2$) are stable with respect to stripes, and narrow rhombi ($\theta = \pi/6$) are unstable. They both bifurcate supercritically. a stripe pattern can never be stable The commonly found pattern with $N = 3$ is the hexagonal pattern, which is also the dominant pattern observed in our PR feedback system near the primary threshold. The nonlinear analysis reveals that only the subcritical branch shows stable patterns. Typically, stripes are unstable in this region, preventing hexagons and stripes to compete.

The situation changes for higher values of the coupling constant Γ. Due to $g_{\pi/3} > g_\pi$, stripes may become stable, and competition may be obtained in this parameter region. Moreover, there exists a secondary threshold $\Gamma_{Sq} \approx 7.20$ at which squares become stable and may coexist with hexagons. As a consequence, a square-hexagon competition can be expected, which involves at least the interaction of $N = 6$ mode pairs. For $N = 6$ modes, typically a steady-state dodecagon branch appears which is described by the Landau

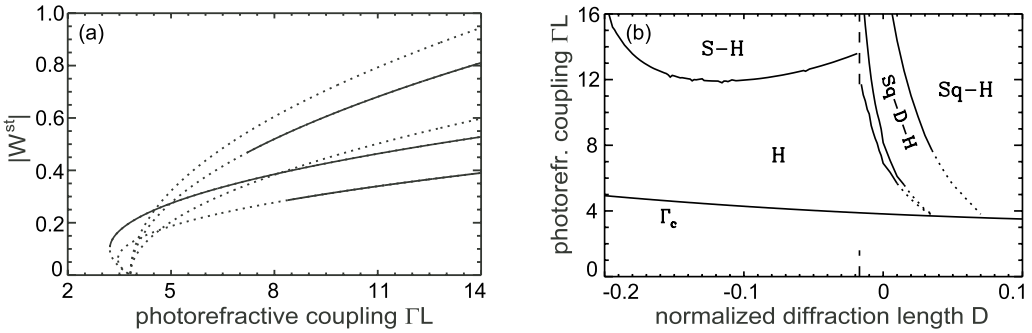

Fig. 4 (a) Amplitude diagram for the substructures of the dodecagonal spot arrangement. H: hexagons, D: dodecagons, S: stripes, Sq: squares, Rh: rhombi. Solid (dotted) lines indicate stable (unstable) branches. (b) Bifurcation diagram showing mono-, bi-, and tri-stability regions. The line Γ_c denotes the appearance of hexagons. S-H and Sq-H are the bi-stability regions, where stripes and hexagons, vis. squares and hexagons coexist. Sq-D-H is the tristability region, where dodecagons may appear in the Sq-H region.

dodecagonal equations. In our PR feedback system, a parameter region emerges at $\Gamma_D \approx 8.39$ in which a stable dodecagonal pattern may appear. Because this pattern contains as subsets both the square and the hexagon spots, it may be simultaneously be stable along with the square-hexagon competition mentioned above. Consequently, tristability is possible. The situation is depicted in Fig. 4, showing the amplitude and bifurcation diagrams of different possibly stable patterns in the PR feedback system.

6 Self-organized patterns in two dimensions

6.1 Gaussian beams

In optics, in contrast to hydrodynamic or ferromagnetic systems, beam profiles are constrained to a finite lateral extent. A laser beam typically has a Gaussian envelope, and the corresponding aspect ratio is small. Therefore, the spatiotemporal attractors in PR wave mixing possess no domain boundaries or front dynamics. At best, defects and their dynamics are observed. A higher aspect ratio can be achieved if the beams are broadened. To accomplish this in our simulations [28], the incident pump beam is chosen as a hyper-Gaussian beam of order 4, while the beam A_2 is determined by what is reflected from the mirror,

$$\begin{aligned} A_1(x,y,0,t) &= \exp[-(x^2+y^2)^4], \\ A_2(x,y,L,t) &= -\sqrt{R}(FT)^{-1}\{\exp(i\phi)\, FT[A_1(x,y,L,t)]\}. \end{aligned} \tag{9}$$

Eqs. (3) and (4) are solved directly, with these boundary conditions. Numerical simulations are performed using a beam-propagation method, augmented by a relaxation-type iteration scheme of second order, to achieve convergence [28]. All simulations are done for $D = 0$, $R = 1$, with the diffraction parameter $f = 0.034$. This corresponds to an aspect ratio of about 20.

The broken inversion symmetry in the PR wave mixing process causes the hexagonal structure to be the preferred pattern in the neighborhood of the primary threshold. Approaching the threshold from below, a hexagonal pattern spontaneously forms out of an initially homogeneous beam profile (Fig. 5). At $t = 80\tau_{\mathrm{PR}}$ a faint unstable ring of active modes becomes visible in the far field. The nonlinear mode interaction breaks the ring into six bean-like spots, which eventually grow to form a hexagon. Higher order modes $\sqrt{3}K_c$ and $2K_c$ gradually appear. This resembles experimental observations [29] of the temporal evolution toward the hexagon state. Owing to critical slowing down, it takes long time to reach the attractor. In the near field, at the output faces of the crystal one recognizes that the hexagonal patterns occur with opposite phases

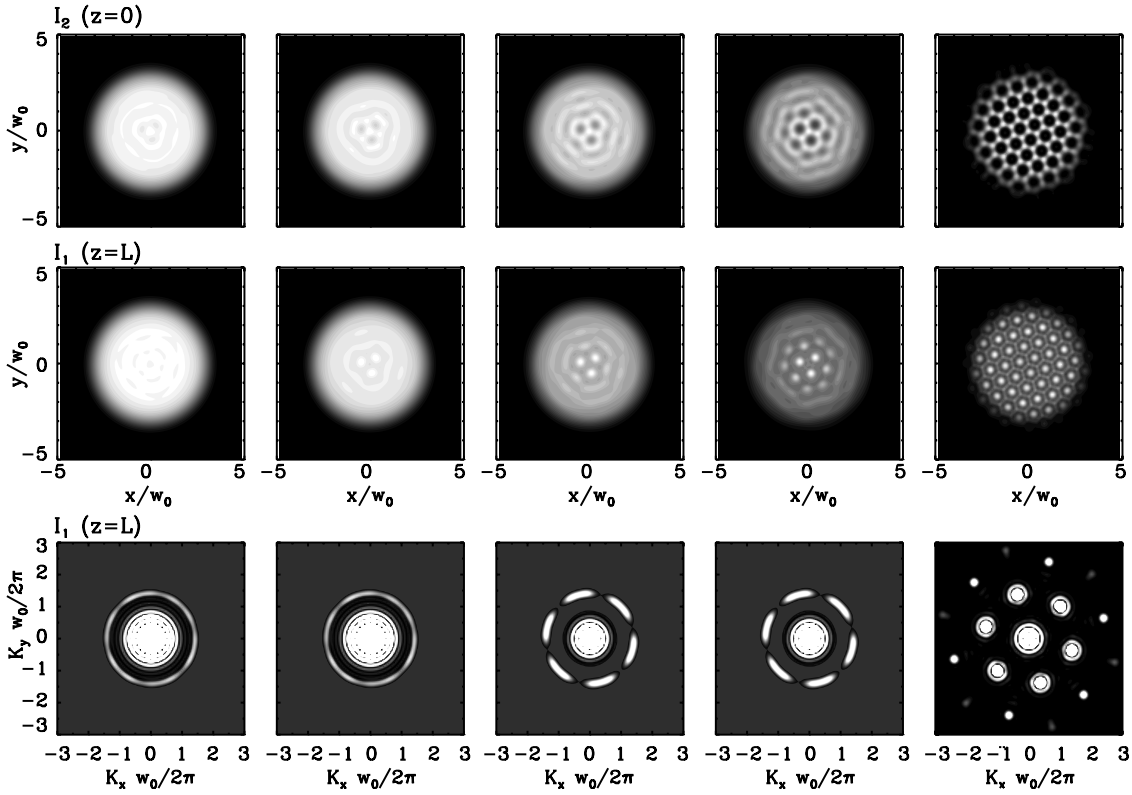

Fig. 5 Temporal evolution of a hexagonal structure out of a homogeneous state, for $\Gamma L = 3.9$. Upper and middle rows, near fields at the crystal faces. Lower row, the corresponding far field. Left-to-right columns: transients at $t/\tau_{\rm PR} = 80, 240, 360, 440$, and the attractor at $t/\tau_{\rm PR} = 2000$.

(Fig. 5). At $z = 0$ the inverted hexagons with the total phase $\Psi = \pi$ appear, whereas at $z = L$ the positive hexagons with $\Psi = 0$ are visible. As mentioned, this is the consequence of broken inversion symmetry at the instability point, which leads to anti-phased patterns being developed.

6.2 Multiple pattern region

Experiments are performed in the geometry introduced in Fig. 1. Over most of the available parameter range, hexagonal patterns are observed above threshold. In this regime, the results of the linear stability analysis are reproduced, albeit with some significant disagreements [12].

The region with negative diffraction lengths is of special interest. A rich variety of different pattern states exists there. In the small parameter region of diffraction lengths $-0.7 \leq D \leq -0.3$, states such as square, squeezed hexagonal, rectangular, rhombic, and even dodecagonal quasiperiodic are observed (Fig. 6) [11]. The patterns are either stable over the observation time, or lose stability to a different pattern on a timescale much larger than the time constant of the system. For the same values of parameters more than one (quasi)stable pattern can be observed, indicating a region of multiple stability. Such regions are known in other physical systems, but have not been observed before in an optical pattern-forming experiment.

In addition to pure patterns, mixed states are observed, in which different patterns coexist and compete on the same or different length scales. The name multiple pattern region appropriately reflects the multitude of patterns observed in this area [12]. Availability of a parameter range with coexisting states naturally suggests the investigation of methods for control and selection of patterns.

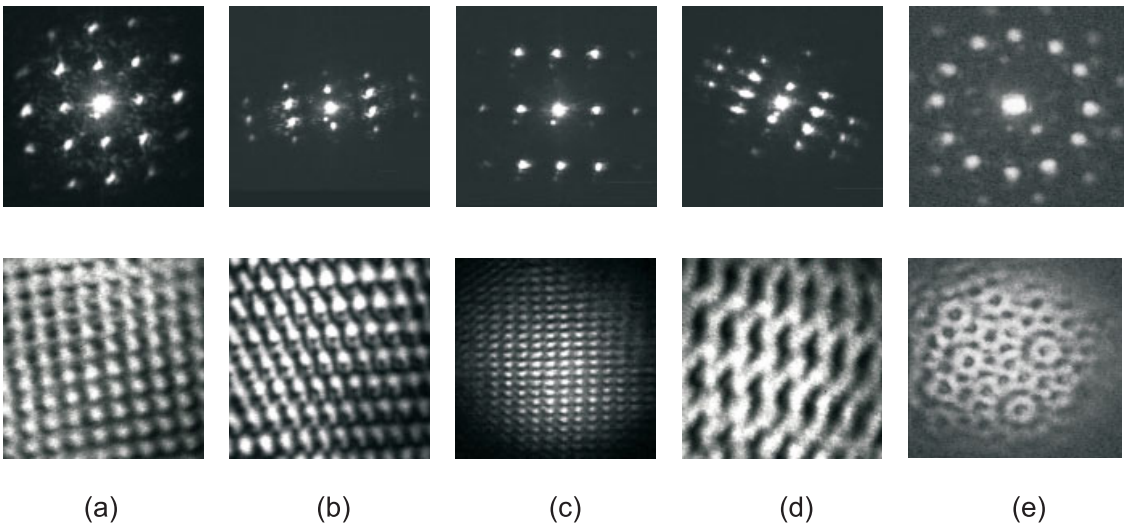

Fig. 6 Examples of the variety of patterns observed in the multiple-pattern region: (a) square, (b) squeezed hexagons, (c) rectangles, (d) rhombi, (e) dodecagons. Upper row: far field, lower row: near field.

7 Control and manipulation of spatial patterns

Selection and stabilization of system solutions which are relatively unstable with respect to another solution is the aim of pattern control. Various applications of control can be envisaged. First, suppression of undesired pattern formation and chaos is necessary to operate optical systems in a highly nonlinear regime required for data transmission purposes. Second, stabilizing one desired state out of many possible is attractive for extending the application of optics to information processing. The potential information capacity of a nonlinear optical system is determined by the total number of different pattern states accessible to the system. Finally, control techniques open the possibility to extract ideal patterns out of noisy experimental pattern and to determine the relative stability of multi-stable solutions, allowing to compare experimental results with the predictions of nonlinear stability analysis. In all cases it is desirable to minimize the influence of the control on the system, so as to retain all the features of the old system – the only difference being an active selection of pattern states.

7.1 Manipulation of spatial patterns in the Fourier domain

Experimentally, the $4f$ imaging system used for the observation of patterns conveniently provides a Fourier plane between the two lenses. Various amplitude masks can be placed into the Fourier plane, to exert influence on the pattern-forming system by selecting or suppressing certain wave numbers, which in turn then will determine the resulting pattern. The basic configuration is given in Fig. 7.

Using this technique, states with defined symmetries and orientation can be addressed. However, as a precondition, the available patterns are still restricted to the ones inherent in the original system. The transverse wave number chosen by the system in the presence of Fourier filter remains unchanged from the case of a free-running system. Three-, five-, or seven-fold symmetric patterns could not be obtained in the experiment, indicating that the chosen patterns have to be members of the family of solutions of the original system.

In experimental implementations as well as in numerical simulations, the method is strongly invasive, as a binary mask alters the mirror boundary conditions, makes the feedback mode-selective and thereby switches some of the active modes to passive ones. To obtain methods that are less destructive to the original system, other approaches are preferred.

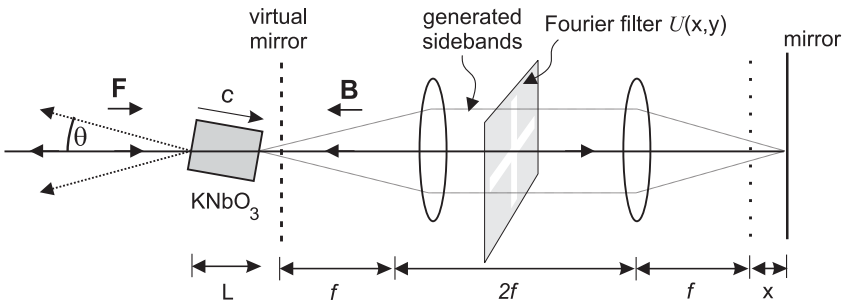

Fig. 7 Experimental configuration for control of patterns using Fourier filters. True mirror distance $x = \frac{1}{n_0} DL$, where L is the crystal length and D the normalized diffraction length.

7.2 Minimally-invasive control of spatial patterns

Activities in non-invasive control of patterns were stimulated by the methods of "chaos control", used to stabilize unstable orbits in temporally chaotic systems. These techniques are based on the requirement that the control signal should tend to zero or ideally vanish as the unstable orbit is reached. To obtain the possibility of definitely changing spatial patterns from one state into another and stabilize unstable spatial patterns it was desirable to extend these methods to spatiotemporal systems. Out of different methods, the manipulation of spatial structures in the Fourier domain has gained widespread success in optics, based on the pioneering work by Martin et al. [30]. The concept is based on the idea to use only a fraction of the original pattern to obtain the control signal. As the PR single feedback system provides regions with multiple stability, it is a natural system to demonstrate the potential of the method [13, 16]. Feedback is provided by two equidistant mirrors in a Michelson-type interferometric geometry [17]. One mirror provides the standard feedback to the nonlinear medium necessary for single feedback pattern formation and contains most of the intensity of the system. The arm containing the second mirror incorporates the control masks in the Fourier plane, transmitting only a small percentage of the total feedback intensity while the central pump beam is blocked. As only a fraction of the total feedback is passed through the mask, the system and its solutions remain essentially unmodified. The term 'minimally invasive' is used, as a certain control signal must remain in order to counter fluctuations induced by noise always present.

The reduced invasiveness of this approach is especially visible using negative control, exploiting the potential of destructive interference in coherent optics: if the optical paths to both mirrors and back are out of phase by π, these components are feed back into the pattern forming system, thereby interfering destructively with the active, undesired modes in the feedback system and weakening them. Therefore, negative control allows for suppression of undesired states. As the system reaches the addressed states, the applied control signal tends to zero (Fig. 8), demonstrating the minimally invasive nature of this technique.

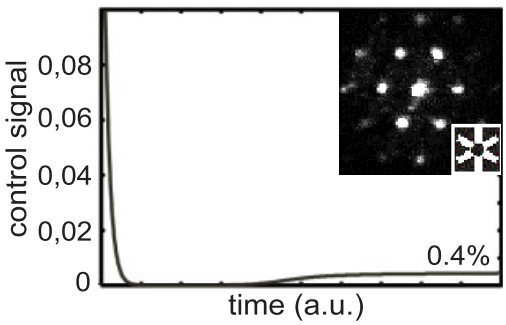

Fig. 8 Example of minimally invasive Fourier filtering. Originally, the orientation of the hexagon was as in Fig. 1. Using the mask (small inset) inhibited the existing pattern by destructive interference and led to a rotated state (as shown). As the system reached the desired state, the total intensity in the control arm (control signal) approached zero. The final value of 0.4% is due to suppression of noise present in the system [3].

8 Conclusions

We have reviewed various aspects of pattern formation and its control in PR systems with a single feedback mirror analytically, numerically and experimentally. Implementing the standard formalism of linear and nonlinear stability analyses to the model equations for wave mixing and the PR nonlinearity, we obtained amplitude equations for the formation of patterns in such a PR feedback system. Owing to the extended nature of the PR nonlinearity, the system not only allows for stable hexagon formation close to the first bifurcation threshold, but also for the formation of squares and consequently for hexagon-square competition. One of the results of this competition is the appearance of dodecagonal as well as a multitude of patterns with two or more different active modes and the appearance of pattern dynamics as well as strong pattern competition effects. Our experimental results exactly demonstrate this behavior in a parameter range, which we name the multiple pattern region.

To determine the relative stability of multi-stable solutions, sophisticated manipulation and control techniques are required. We presented results of different concepts of Fourier control of PR patterns, allowing to control the patterns without changing the states of the system. These techniques are important for potential applications of pattern formation in information processing. On the one hand, they provide suppression of undesired pattern formation and chaos, and allow the operation of optical systems in a highly nonlinear regime required for data transmission purposes. Second, stabilizing one desired state out of many possible is attractive for system that are based on self-organized pattern search or associative features in highly connected optical network systems.

Acknowledgements Work at the Institute of Applied Physics, WWU Münster is partially supported by Deutsche Forschungsgemeinschaft, under contract De 486-10. Work at the Universite Libre de Bruxelles was supported by the IAP program of the Belgian government.

References

[1] F. T. Arecchi, S. Boccaletti, and P. L. Ramazza, Phys. Rep. **318**, 1 (1999).
[2] R. Neubecker and T. Tschudi (eds.), Chaos Solitons Fractals **10** (1999).
[3] C. Denz, M. Schwab, and C. Weilnau, Transverse Pattern Formation in Photorefractive Optics, (Springer, Berlin, 2003).
[4] K. Staliunas and V. Sanchez-Morcillo, Transverse Patterns in Nonlinear Optical Resonators (Springer, Berlin, 2003).
[5] M. Saffman, A. A. Zozulya, and D. Z. Anderson, J. Opt. Soc. Am. B **11**, 1409 (1994).
[6] T. Honda, Opt. Lett. **18**, 598 (1993).
[7] T. Honda, Opt. Lett. **20**, 851 (1995).
[8] T. Honda and H. Matsumoto, Opt. Lett. **20**, 1755 (1995).
[9] T. Honda and P. P. Banerjee, Opt. Lett. **21**, 779 (1996).
[10] A. V. Mamaev and M. Saffman, Europhys. Lett. **34**, 669 (1996).
[11] T. Honda, H. Matsumoto, M. Sedlatschek, C. Denz, and T. Tschudi, Opt. Commun. **133**, 293 (1996).
[12] M. Schwab, C. Denz, and M. Saffman, Appl. Phys. B **69**, 429 (1999).
[13] S. Juul Jensen, M. Schwab, and C. Denz, Phys. Rev. Lett. **81**, 1614 (1998).
[14] C. Denz, M. Schwab, M. Sedlatschek, T. Tschudi, and T. Honda J. Opt. Soc. Am. B **15**, 2057 (1998).
[15] M. Schwab, M. Sedlatschek, B. Thüring, C. Denz, and T. Tschudi, Chaos Solitons Fractals **10**, 701 (1999).
[16] A. V. Mamaev and M. Saffman, Phys. Rev. Lett. **80**, 3499 (1998).
[17] M. Schwab, M. Saffman, C. Denz, and T. Tschudi, Opt. Commun. **170**, 12 (1999).
[18] C. Denz, S. Juul Jensen, M. Schwab, and T. Tschudi, J. Opt. B **1**, 114–120 (1999).
[19] M. Schwab, C. Denz, A. Mamaev, and M. Saffman, J. Opt. B **3**, 318–327 (2001).
[20] Yu. A. Logvin, Phys. Rev. A **57**, 1219 (1998).
[21] A. Ashkin, G. D. Boyd, J. M. Dziedzic, R. G. Smith, A. A. Ballman, J. J. Levinstein, and K. Nassau, Appl. Phys. Lett. **9**, 72 (1966).

[22] P. Günter and J.-P. Huignard, Photorefractive Materials and their Applications (Springer Verlag, Berlin, 1988, 1989).
[23] L. Solymar, D. J. Webb, and A. Grunett-Jepsen, The Physics and Applications of Photorefractive Materials (Clarendon Press, Oxford, 1996).
[24] N. V. Kukhtarev, V. B. Markov, S. G. Odulov, M. S. Soskin, and V. L. Vinetskii, Ferroelectrics **22**, 949 (1979).
[25] P. P. Banerjee, H. Yu, D. A. Gregory, N. Kuhktarev, and H. J. Caulfield, Opt. Lett. **20**, 10–12 (1995).
[26] M. Saffman, A. A. Zozulya, and D. Z. Anderson, J. Opt. Soc. Am. B **11**, 1409 (1994).
[27] A. I. Chernyikh, B. I. Sturman, M. Aguilar, and F. Agullo-Lopez J. Opt. Soc. Am. B **14**, 1754 (1997).
[28] O. Sandfuchs, F. Kaiser, and M. R. Belić, Phys. Rev. A **64**, 063809 (2001).
[29] S. G. Odoulov, M. Y. Goulkov, and O. A. Shinkarenko, Phys. Rev. Lett. **83**, 3637 (1999).
[30] R. Martin, A. J. Scroggie, G. L. Oppo, and W. Firth, Phys. Rev. Lett. **77**, 4007 (1996).